JAAS

ROYAL SOCIETY OF CHEMISTRY

PAPER

View Article Online
View Journal

Cite this: DOI: 10.1039/d6ja00144k

Less is more: how reducing the ablation atmosphere pressure can boost sensitivity for fluorine in laser-induced breakdown spectroscopy

David Ken Gibbs and Andreas Limbeck *

Laser-induced breakdown spectroscopy (LIBS) is a rapid and minimally destructive technique which enables measurement of almost every element of the periodic table. However, fluorine determination remains challenging due to low sensitivity and weak emission signals. In this work, the influence of reduced ablation atmosphere pressure on fluorine detection by LIBS is systematically investigated, including parameter optimization steps for gate delay and laser energy. A significant increase in fluorine signal intensity was observed with decreasing pressure. The impact of pressure on signal stability, calibration behaviour, and limits of detection was assessed and compared to measurements at atmospheric pressure. In that regard, different evaluation approaches, including univariate and multivariate models (using Partial Least Squares) were considered. The results demonstrate that reduced-pressure conditions lead to improved sensitivity and lower limits of detection, enabling more reliable fluorine quantification. For the univariate calibration models, sensitivity was approx. double at 50 mbar compared to atmospheric pressure, while the limit of detection reduced from 505 to 104 μg g^{-1}. Further, sensitivity in the multivariate models improved by up to 80% leading to a decreased limit of detection of 121 μg g^{-1} at 50 mbar in comparison to 286 μg g^{-1} at atmospheric pressure. The findings presented here show that controlling the ambient pressure is an effective strategy to enhance fluorine detection by LIBS without requiring extensive sample preparation or major instrumental modifications. This approach broadens the applicability of LIBS for the direct analysis of fluorine in solid samples and provides a practical route to improved analytical performance.

Received 20th April 2026
Accepted 27th May 2026

DOI: 10.1039/d6ja00144k

rsc.li/jaas

1. Introduction

The analysis of fluorine (abbreviated as F from here on), in particular that of per- and polyfluoroalkyl substances (PFAS), is currently a highly active field of research. This is largely premeditated by regulatory pressure to limit the exposure of the general public to PFAS and related substances due to adversary health effects. Most of the compounds that fall under the broad definition of PFAS (encompassing at least 10 000 substances) either directly pose risks or degrade into substances that are harmful as a result of very high persistence, mobility, (bio) accumulation, (eco)toxicity, and direct effects on human health. Consequently, several countries and institutions are trying to or have already implemented measures to reduce PFAS concentrations, especially in consumer products.[1]

At the time of writing, the European Union is intending to impose restrictions on the PFAS and general F content of any substance, mixture, or article placed on European markets. Additionally, the current draft of the European Chemicals Agency (ECHA) for the universal PFAS restriction defines an information requirement for products containing more than 50 μg g^{-1} of total F, requiring the manufacturer, importer, or downstream user to prove whether the F content is a result of PFASs or other fluorinated compounds.[1]

To assess the total F content, techniques such as Combustion Ion Chromatography (CIC,[2]), High-Resolution Continuum Source Molecular Absorption Spectrometry (HR-CS-MAS,[3]), Ion Selective Electrode (F-ISE,[4]), and Particle-induced Gamma-ray Emission (PIGE,[2]) are commonly applied,[1,5] but come with limitations. For instance, CIC requires an extraction, combustion, and chromatography step, limiting sample throughput. HR-CS-MAS instruments are limited to single-element and bulk analyses and also not widely used in analytical laboratories. F-ISE is confined to determining the concentration of ionic F^- in solution, which requires the prior conversion of solid samples into solutions suitable for analysis. PIGE is a surface-limited technique (probing a shallow and fixed depth of several tens of μm) and requires access to particle accelerators. In this context, Laser-Induced Breakdown Spectroscopy (LIBS) could serve as an alternative to the aforementioned techniques, which is not strictly limited to bulk analysis and typically does not require sample preparation, enabling a direct and fast analysis of the finished product.

TU Wien, Institute of Chemical Technologies and Analytics, Getreidemarkt 9/164, 1060, Vienna, Austria. E-mail: andreas.limbeck@tuwien.ac.at

An additional advantage of LIBS is that it can operate in air and at atmospheric pressure, but usually samples are placed in an ablation chamber that is flushed with an inert gas (*e.g.*, He or Ar), which affects both intensity and emission line width. In this context, Ar generally delivers the highest intensity, plasma temperature, and electron density, whereas He provides the better signal-to-noise ratio.[6,7] For F, the impact of the composition was studied by, *e.g.*, Tran *et al.*[8] as well as Cremers and Radziemski,[9] who both found that He lead to a better limit of detection (LOD). Not only the composition, but also the pressure of the ablation atmosphere significantly affects the LIBS spectrum. Scott, Effenberger, and Hatch provide a general overview of the impact of the ablation atmosphere, where they conclude that reduced ablation atmosphere pressures "tend to improve LIBS spectra by increasing the intensity or [signal-to-noise ratio] and improving resolution."[7] However, to the best of our knowledge, a study investigating the impact of the ablation atmosphere pressures has not been performed for F.

While LIBS is a technique that can detect most elements with appreciable LODs in the low $\mu g\ g^{-1}$ range, this does not typically apply to F, at least in condensed matter. For example, in 2014 Quarles *et al.*[10] reported a LOD of 135 $\mu g\ g^{-1}$ for the atomic F I emission line in geological samples, whereas Cremers and Radziemski[9] provide a value of just 38 $\mu g\ g^{-1}$ based on SF_6 gas in He atmosphere as early as 1983. This disparity can by and large be explained by the so-called matrix effect, which inherently limits quantification in LIBS. The reasons for the poor sensitivity for F have been discussed in detail in the literature, *e.g.*, ref. 10–12. In short, the most intense emission lines of F lie in the usually not accessible VUV spectral range (<190 nm), the excitation and ionization efficiency of F in He and Ar atmospheres are low, and the most intense emission in the UV/vis range (at ~685.6 nm) has weak intensity due to its high upper energetic level.[13] Detecting the molecular emissions instead of the atomic F emission has significantly improved LODs. Using this approach, Quarles *et al.*[14] recently reported a LOD as low as 4 $\mu g\ g^{-1}$.

Even so, a further complication for the analysis of F is the investigated sample matrix. In the literature, F analysis with LIBS is mainly focused on geological samples[10,12,14,15] or pressed powders.[11,13,16] To the best of our knowledge, a study on the quantification of F in a polymeric matrix with LIBS has not been reported before, despite two recent publications from our group also discussing the analysis of F in polymers. However, Weiss *et al.*[17] mainly dealt with the comparison of the molecular emissions of CaF and CuF, concluding that the latter resulted in a lower LOD based on pressed powder standards of a mixture of cellulose and PTFE. Additionally, Brunnbauer *et al.*[18] demonstrated that PTFE particles embedded in acrylic resin could be detected with a spot size of 5 × 5 μm, allowing for the identification of the particles in an imaging experiment. It has to be considered, however, that PTFE has a theoretical F content of 0.76 $g\ g^{-1}$, raising questions about comparability due to the matrix effect. More precisely, it can be appreciated that the large majority of C in the samples may reduce the emission intensity as a result of a chemical matrix effect.[19] Moreover, Bonta and Limbeck[20] found that notable sensitivity differences for metals exist even between polymers.

Here we investigate polymer matrices, more specifically polyimides (PIs). PIs are a class of high-performance polymers that commonly exhibit high thermal stability, mechanical toughness, chemical resistance, and dielectric integrity. They are usually formed from soluble poly(amic acid) precursors, which are a combination of dianhydrides and diamines, by a chemical or thermal process, yielding films or fibers, for instance. One of the key advantages of polyimides is their versatility, resulting in a variety of possible property enhancements such as higher adhesion or hydrolytic stability as well as lower water absorption. Adhesion and transparency make PI thin films an ideal candidate for coating applications in industries such as sensors, automotive, spacecraft, metallurgy, membranes, microelectronics, electrical devices/packaging, and optics.[21–24]

While conventional polyimides (*e.g.*, Kapton®) do not contain F in their polymer structure, the introduction of F increases solubility and processability, while decreasing water absorption and dielectric constant, with the improvements being directly linked to the F content.[24] Even if no F is present in the polyimide itself initially, fluoropolymers may be used as adhesives for coating purposes,[21] or fluorinated compounds may be utilized as fillers,[24] potentially leading to (intentional) F content in the polyimide.

In this work, we want to provide an in-depth investigation into the detection of F in a polymer matrix with LIBS (where F is a trace component) and the concomitant difficulties when working close to the detection limit. Initially, the focus is on method development and the impact of ablation atmosphere pressure on the resulting spectra. The second part starts with a discussion on data processing procedures to arrive at meaningful values to use for calibration, followed by a comparison of the different metrics and their performance. We specifically focus on the LOD and evaluate alternative definitions (different to the conventional formula accepted by the International Union of Pure and Applied Chemistry (IUPAC)) to demonstrate the conflict between the calculated value and a "practical", more conservative LOD.

2. Experimental

2.1 In-house polymer film preparation

All method development was carried out using in-house produced polymer thin films based on PI. First, the polyimide P84 (200 mesh, Ensinger Sintimid, Lenzing, Austria) in powder form was dissolved in *N*-methyl-2-pyrrolidone (short: NMP, 99.5%, abcr GmbH, Karlsruhe, Germany) to obtain a polymer concentration of approx. 250 $mg\ g^{-1}$ in the solution. Then, a F stock solution was produced by dissolving sodium trifluoromethanesulfonate (98%, Thermo Fischer (Kandel) GmbH, Kandel, Germany) in NMP before preparing a dilution series by diluting the stock solution or dilutions with NMP. Next, aliquots of the polymer solution were combined with the dilutions before subjecting them to the subsequent spin-coating process. Blank standards were subjected to the same

procedure, though instead of adding a F-containing solution, NMP was added to the polymer solution aliquot instead.

To create polymer films that are reasonably even (apart from the edge) and thin, but still thick enough for LIBS analysis, spin-coating the spiked polymer solutions onto Si wafer pieces (high-purity, n-doped, cut to 1 cm by 1 cm pieces) provided by Infineon Austria AG (Villach, Austria) was elected as preparation technique. The spin coater used here was the SPC8-HC by Mendel Chemicals SRL (Chisinau, Moldova) and parameters that were optimized included initial polymer concentration, the rotational frequency, as well as the applied volume of the solution. Ultimately, the concentration of 250 mg g^{-1} mentioned earlier, a rotation speed of 3000 rpm and a volume of 100 μL were identified as optimal while performing static spin coating, *i.e.*, the solution was applied to the wafer before starting the spinning step. Afterwards, the wafer pieces were transferred to a hot plate set to 100 °C for 5 min to evaporate the solvent. After this step, the final nominal F concentration in the polymer films used for calibration ranged from 0 to 2000 μg g^{-1}. This is based on the assumption that the solvent evaporates quantitatively, meaning that the concentration of F in the polyimide film resulted from the initial weights of the F-containing solution and the polyimide solution.

The film thickness was evaluated by mechanical profilometry with a Dektak XT (Bruker, Billerica (MA), USA) by rupturing several equally prepared films in the center of the wafer pieces and measuring the height of the step between areas with and without polymer coating. An approximate thickness of 7 μm was determined this way, which was sufficiently thick to not be ablated within one pass during LIBS analysis.

2.2 Sample description

Polyimide film samples (denoted PI 1 through PI 7) were provided by an industrial partner and represent polyimides in development intended as encapsulation/coating material for products in the semiconductor industry. They were generally received as (industrially) spin-coated on Si wafers as substrate. The wafers were manually broken into smaller pieces to fit inside the ablation chamber, but were otherwise measured as is. Furthermore, during method development the NIST SRM610 and NIST SRM612 (Gaithersburg (MD), USA) were analyzed to assess the applicability of the approach to different matrices.

2.3 LIBS instrumentation and sample analysis

LIBS measurements were performed using a combination of a LIBS J200 system (Applied Spectra, Inc., Fremont (CA), USA) and a detection unit comprised of a SpectraPro HRS-750 MS spectrograph and a PI-MAX4 (1024 × 256) ICCD camera (both Teledyne Princeton Instruments, Acton (MA), USA), where the PI-MAX4 was connected directly to the exit port of the SpectraPro HRS-750 MS.

The LIBS J200 system featured a frequency-quadrupled, Q-switched Nd:YAG laser using a wavelength of 266 nm with a 5 ns pulse width, optimized for operation at 20 Hz. Radiation emitted from the laser-induced plasma was collected by one of the built-in collection optics, which is situated at a 45° angle relative to the beam path in a fixed position approx. 10 cm away from the ablation crater. The output of the collection optic was connected to a BFL200HS02 fiber (Thorlabs GmbH, Munich, Germany), a round-to-linear fiber bundle of 2 m length containing 7 fibers with a 200 ± 4 μm core diameter (certified for a wavelength range of 250 to 1200 nm), which in turn was connected to the input of the SpectraPro HRS-750 MS spectrograph's universal fiber coupler input. To ensure proper alignment of the linear end of the fiber with the entrance slit of the spectrograph, the universal fiber coupler was rotated to achieve maximum intensity for the Ca I emission at ∼458.3 nm when ablating the NIST SRM612 during performance tuning.

In order to achieve an ablation atmosphere pressure below atmospheric pressure, a custom-built ablation chamber (Huber Scientific, Vienna, Austria) was used, which was described previously in ref. 25. In short, it allows for the control of the ablation atmosphere pressure when attaching the gas outlet to a laboratory vacuum pump, which in this case was a LVS 110 Tp ecoflex (ILMVAC GmbH, Ilmenau, Germany). When using He as ablation atmosphere the pressure could reasonably be set as low as ∼35 mbar.

The SpectraPro HRS-750-MS was a Czerny–Turner spectrograph with a focal length of 750 mm and contained a turret with different gratings, though for this work only the grating with a density of 1800 g mm^{-1} and a blaze of 500 nm was used. Furthermore, the PI-MAX4 ICCD camera consisted of a gap-less 1024 × 253 pixel array with each pixel having a width and height of 26 μm, respectively. Of this array, a rectangular, so-called "region of interest" with a width of 685 (of 1024) pixels and a height of 76 (of 253) pixels in the center of the detector was selected, where the 76 pixels perpendicular to the wavelength separation axis were binned. According to the manufacturer's specification, the HRf filmless Gen III intensifier coating allowed for sensitive measurements in the range of 350 to 950 nm. The detector was cooled to −20 °C by the built-in cooling system. All in all, when measuring the atomic F I emission at ∼685.7 nm, this detection setup allowed for the recording of spectra with a spectral width of ∼9.352 nm and an average wavelength spacing in this range of ∼0.014 nm.

Instrumental variables, which remained constant throughout the investigation, include: (1) He as ablation atmosphere; (2) laser spot size of 100 μm set for the LIBS J200; (3) scan speed of 1 mm s^{-1}, which combined with 20 Hz laser frequency and of 100 μm laser spot size meant that shots were overlapped by half the laser spot diameter; (4) (entrance) slit width of 400 μm of the HRS-750-MS; (5) center wavelength of 687 nm of the HRS-750-MS; (6) intensifier gain of 20 of the PI-MAX 4.

2.4 Data evaluation

The LIBS J200 system was controlled by the software provided by the manufacturer (Axiom version 2.0), while the LIBS spectra were acquired using Lightfield® (Teledyne Princeton Instruments, version 6.13.1.2008) using the Q-switch trigger signal from the LIBS J200 system as the external trigger source. The

SPE files generated by Lightfield® were then evaluated by self-developed Python scripts (see Section S1 of the SI).

3. Results and discussion

The main aim of this work is to demonstrate the influence of a reduction in ablation atmosphere pressure on the signal of F. More precisely, we examine the spectral changes that come with pressure modulation as well as the effect of different data treatments on the subsequent evaluation and performance metrics (*e.g.*, sensitivity and LOD). Furthermore, we highlight the challenges related to quantifying F in polymer matrices with LIBS at the lower μg g^{-1} level and discuss possible reasons for this behavior, before providing a reasonable estimate for the limit of detection.

As a reference point, Fig. 1 illustrates spectra obtained at atmospheric pressure from three repeat measurements of the PI film standard with no added F. What is immediately clear from looking at the full spectra in Fig. 1a, is that the baseline is markedly jagged. Apart from the C I emission at approx. 682.8 nm, there are several features that could not be assigned to an element with known content in the PI with the NIST Spectral Database.[26] When observing the zoomed-in wavelength region of the most intense F I emission in the measured wavelength range in Fig. 1b the spectra exhibit a clear emission peak, which cannot fully be attributed to F, because the wavelength shift and peak width are too large.

To the best of our knowledge, LIBS studies on polymers that focus on this particular spectral range are not available in the literature. While there are several works that investigate the molecular CN and C2 emissions in depth (*e.g.*, Gajarska *et al.*,[27] Trautner *et al.*,[28] Chamradová, Pořízka, and Kaiser[29]), these emissions do not fall in the investigated wavelength range. Hence, to judge whether the background is systematic and/or unique to PI, other polymers were analyzed with the same acquisition parameters. The spectra comparison and further discussion can be found in SI Fig. S1 and Section S2, respectively. All things considered, we assume that the background visible in this spectral range corresponds to molecular emissions from the polymer, which are detected mainly due to the use of an ICCD detector with a moderately high intensifier gain setting combined with the low wavelength spacing of the spectrograph.

3.1 Parameter optimization: laser energy and ablation atmosphere pressure

Generally, signal intensity in LIBS can be boosted by increasing the pulse energy of the incoming laser radiation, given that more material is vaporized and the laser-induced plasma then contains more emitting species. The maximum usable pulse energy for the experimental setup was approx. 8.21 mJ per pulse (as determined by an external power meter). Even though the LIBS J200 system allowed for higher pulse energies, significant degradation of the optical window (of the custom-built ablation chamber) was observed over time, which is why it was decided to limit the power output.

In Fig. 2, a reduced wavelength range of the spectra of a PI film standard with 2145 μg g^{-1} added F are compared for different laser energies and ablation atmosphere pressures. The full spectra as well as the zoomed-in region of the most intense F I emission are provided in SI Fig. S3. Evidently, the reduction in ablation atmosphere pressure resulted in a decrease of overall intensity for all laser energies. However, it is clear that the intensity corresponding to the F I emission was enhanced absolutely (and relative to the surrounding), with the effect being especially pronounced for lower laser energies. Irrespective of the pressure, an increase in laser energy lead to a boost in signal intensity for F, while simultaneously elevating the overall intensity.

To assess the evolution of the spectra with changing experimental parameters, three evaluation metrics were calculated. In the following, the sum intensity within 685.4–685.9 nm after background correction (*cf.* chapter 3.4) is referred to as the signal (intensity). The average intensity within 686.4–686.7 nm – corresponding to 22 spectral data points – was employed as the

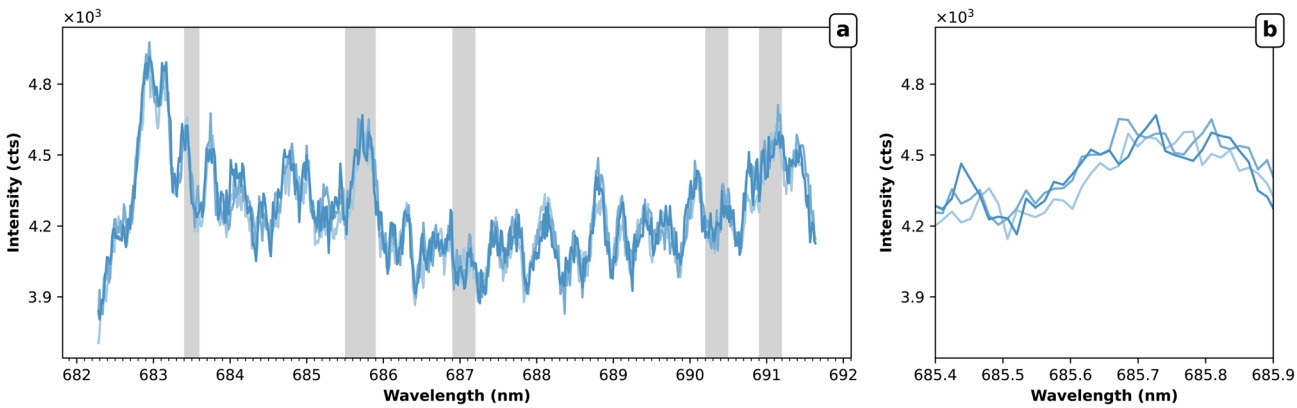

Fig. 1 LIBS spectra (three repeat measurements) obtained from a PI film with no added F. The shaded areas mark wavelength regions with significant F I emission in the measured wavelength range (according to the NIST Atomic Spectra Database[26]). (a) shows the full spectra, whereas as (b) focuses on the region of the most intense F I emission line. Spectra were acquired at atmospheric pressure with a laser energy of 8.21 mJ, gate delay of 0.4 μs, and gate width of 2.0 μs and resemble the average spectrum of 42 laser shots.

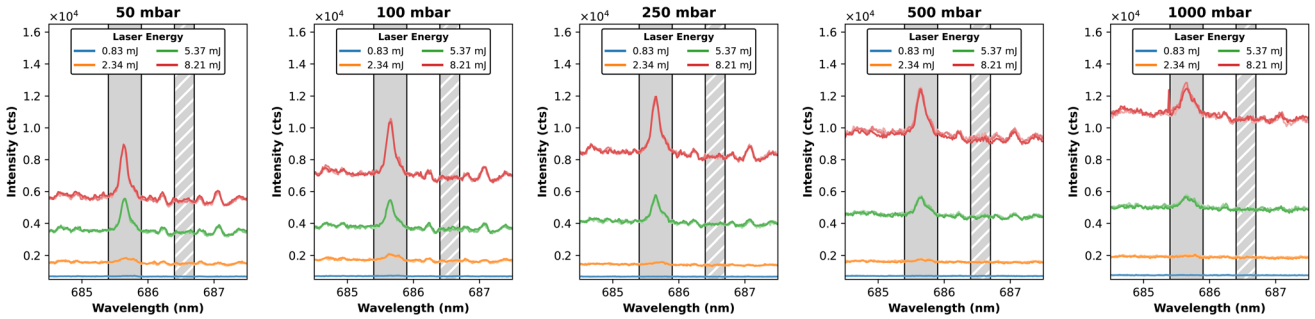

Fig. 2 Comparison of spectra for different laser energies and ablation atmosphere pressures. The fully shaded area highlights the wavelength region used to calculate the signal (685.4–685.9 nm), whereas the striped area marks the region employed for background and noise calculation (686.4–686.7 nm). Spectra represent the average of 42 shots from the analysis of a standard containing 2145 μg g^{-1} F, acquired with a gate delay of 0.3 μs and a gate width of 5.0 μs. The five repeat measurements of each laser energy use the same base color, but different opacity.

background. We found that this wavelength range was generally feature-less and showed no dependency on the ablation atmosphere pressure, laser energy, and gate delay (as shown later) apart from a change in absolute intensity. The metric that is derived by dividing the maximum intensity of the F I emission at ~685.7 nm by the background is denoted as the signal-to-background ratio (SBR). Additionally, to estimate the variation of the background, the standard deviation of the intensity within 686.4–686.7 nm is assumed to be indicative of the noise of the measurement.

Fig. 3 illustrates the dependence of the signal intensity, noise, and signal-to-background ratio for four different laser energies (0.83 mJ to 8.21 mJ) and five ablation atmosphere pressures (50 mbar to 1000 mbar). From Fig. 3a it is obvious that the raised pulse energy favors signal intensity, even after subtracting a local linear baseline (*cf.* Section 3.4). Interestingly, the sum intensity in the range of the most intense F I emission actually decreases for the highest laser energy for pressures below 250 mbar, while it increases further for the other energies. On the contrary, the SBR depicted in Fig. 3c, steadily improves for 8.21 and 5.37 mJ regardless of pressure, but is slightly reduced for 2.34 and 0.83 mJ at 50 mbar compared to 100 mbar. Moreover, the noise exhibits no clear trend with pressure, but is elevated with higher laser energy. The latter is expected since the augmented background leads to higher absolute values for the standard deviation.

The observed trends are comparable to literature. For instance, Iida found that the intensity of the Fe I emission at 374.949 nm showed a maximum at approx. 300 Torr in a He atmosphere using a Nd:YAG laser with a pulse energy of 120 mJ and a spot size of 0.4 mm, though not explicitly providing figures for the signal-to-background ratio.[30] Yalçın, Tsui, and Fedosejevs found in their investigation with a Ti:sapphire laser with 10 μJ pulse energy and 28 μm spot size that the emission of Al I (as well as Mg, Fe and Cu) was significantly higher at a pressure of 4 Torr compared to 760 Torr for an air

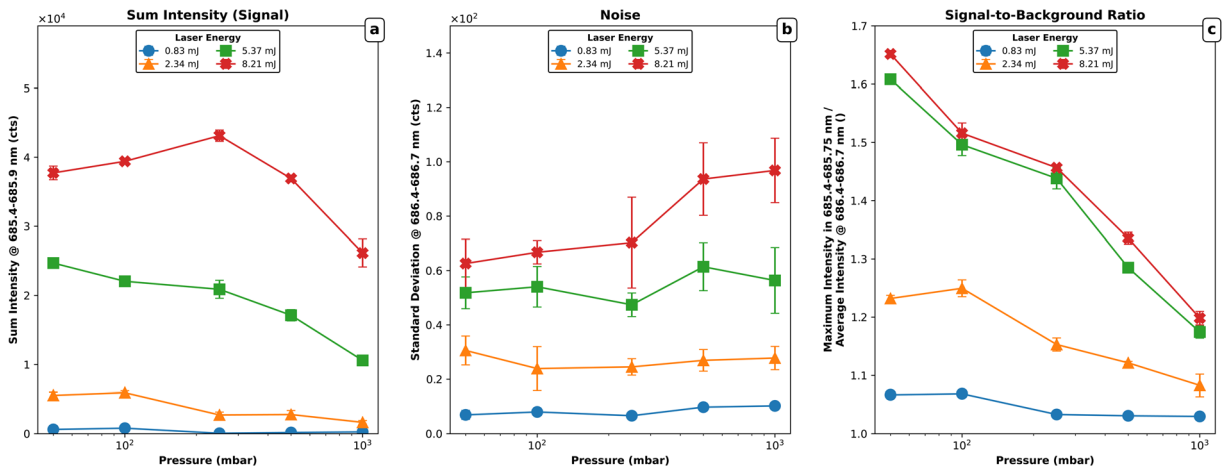

Fig. 3 Comparison of metrics for different energies and ablation atmosphere pressures. (a) Sum intensity around the most intense F I emission line in the investigated spectral range (685.4–685.9 nm, local background subtraction). (b) Noise, determined as the standard deviation in a region of 686.4–686.7 nm. (c) Signal-to-background ratio, calculated by dividing the maximum within 685.4–685.75 nm by the average intensity within 686.4–686.7 nm. Spectra used for evaluation (see SI Fig. S3) resemble the average of 42 shots from the analysis of a standard containing 2145 μg g^{-1} F, acquired with a gate delay of 0.3 μs and a gate width of 5.0 μs. Error bars represent the standard deviation of five repeat measurements.

atmosphere.[31] Furthermore, they noted that the noise around the emission peak of Al I was almost constant regardless of pressure. In their review, Scott, Effenberger and Hatch summarize that reduced pressures enhance LIBS spectra by increasing intensity and/or signal-to-noise ratio as a consequence of reduced plasma shielding, resulting in more ablation and less Stark broadening because of lower electron density.[7]

To determine whether the improvement in signal intensity may stem from an elevated ablation rate of the polymers under reduced pressure profilometric measurements were carried out. A comparison of different ablation atmosphere pressures and energies (complemented by the evaluation procedure) is provided in Section S3 of the SI and shows that the ablation depth is identical for 50, 250, and 1000 mbar, independent of the employed laser energy. This principally contradicts the findings of, for instance, Wu *et al.*,[32] Vadillo *et al.*,[33] and Iida,[30] who found a dependency of the crater depth or ablation rate on ablation atmosphere pressure. However, it has to be considered that these works analyzed metal surfaces as opposed to polymers. Regardless, it is clear that an increase in laser energy resulted in higher ablation rates, correlating with a boost in detected signal intensity.

3.2 Parameter optimization: gate delay and ablation atmosphere pressure

Depending on the gate delay and gate width, the laser-induced plasma emission transitions from initially mainly non-characteristic continuum radiation to contributions of discrete ionic, atomic, and molecular emissions that are characteristic for the sample's constituents.[34] Since the emission of F in the investigated spectral range is of atomic nature, the fundamental challenge is to attenuate the continuum radiation, whilst not diminishing F I intensity.

Several works have dealt with optimizing the gate delay for the F I emission. Measuring gases and/or aerosols in air with Nd:YAG laser at 1064 nm, Cremers and Radziemski determined an optimal delay of ~1 μs,[9] whereas Williamson *et al.* noted that the optimum could be at up to 20 μs, depending on the analyte.[35] In condensed matter, the gate delay tends to be lower. Gondal *et al.* report an optimum at 0.7 μs for toothpaste samples employing a fourth harmonic Nd:YAG laser at 266 nm with a pulse energy of 50 mJ and a spot size of 100 μm.[36] Quarles *et al.* mention that they achieved the best signal-to-background ratio with a gate delay as low as 0.2 μs for a LIBS J200 system with a 213 nm Nd:YAG laser.[10]

To determine the optimal gate delay, so-called kinetic series were conducted by closely following the approach of Gaft *et al.*[12] A kinetic series describes a set of measurements in which the gate delay is continuously increased, while keeping the gate width and other instrumental parameters constant. An alternative term used by, *e.g.*, Moon, Smith, and Omenetto is the line-to-continuum approach.[37] Analogous to Section 3.1, the goal was to maximize signal intensity and the signal-to-background ratio and to investigate the impact of pressure on performance metrics. Fig. 4 shows the spectral changes introduced by increasing the gate delay at different pressures, using a constant gate width of 0.5 μs in a reduced wavelength range. The full spectra are illustrated in SI Fig. S4. With increasing gate delay the overall background intensity significantly decreases. At the same time, the signal intensity diminishes too; at 1.8 μs the peak of the F I emission at ~685.7 nm cannot be

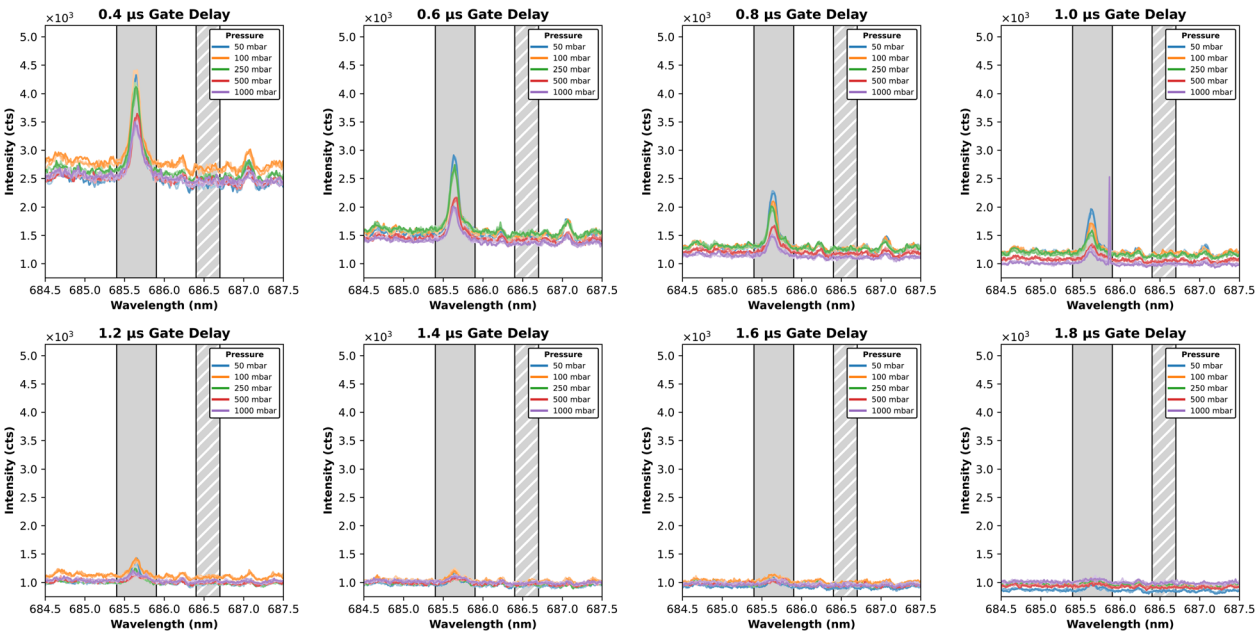

Fig. 4 Comparison of spectra for different gate delays and ablation atmosphere pressures. The fully shaded area highlights the wavelength region used to calculate the signal (685.4–685.9 nm), whereas the striped area marks the region employed for background and noise calculation (686.4–686.7 nm). Spectra represent the average of 42 shots from the analysis of a standard containing 2145 μg g^{-1} F, acquired with a gate width of 0.5 μs. The five repeat measurements of each laser energy use the same base color, but different opacity.

distinguished from the surrounding background. However, for all gate delays a boost in signal intensity with decreasing ablation atmosphere pressure can be observed. Depending on the gate delay, the peak intensity compared to the base is approx. doubled or tripled at 50 mbar in relation to atmospheric pressure. Furthermore, Fig. 4 reaffirms the suitability of the region at 686.4–686.7 nm to resemble the background intensity, since it is not affected by a change in gate delay and pressure apart from the absolute intensity.

Fig. 5 compares the sum intensity, noise, and SBR for the different ablation atmosphere pressures and gate delays at a constant gate width of 0.5 μs. As expected, the sum intensity steadily declines with increasing gate delay. With a reduction in ablation atmosphere pressure the signal intensity increases for a given gate delay, but interestingly, at larger gate delays the intensity assumes a similar value regardless of pressure. The noise, *i.e.*, the standard deviation of the background, decreases with increasing gate delay, mainly as a result of the absolute intensity being lower. Fig. 5c indicates that an optimum of the SBR can be obtained at a gate delay of 0.6 μs for all pressures.

Surprisingly, the overall background intensity is comparable for all pressures from a gate delay of 0.4 μs onwards. This is in stark contrast to the data obtained for a gate delay of 0.2 μs, which is depicted in SI Fig. S5, where the background for 1000 mbar is almost a factor of two higher than for 50 mbar. Similar findings were reported by Wu *et al.*[32] for the W I emission of a pure tungsten target (in air) using a 1064 nm Nd:YAG laser, indicating that the continuum decays faster at a reduced pressure. Scott, Effenberger, and Hatch explain that this is a result of reduced electron density at lower pressure, leading to less continuum radiation.[7] All in all, it was concluded that a gate delay of approx. 0.4 μs was optimal and we chose a gate width of 2.0 μs to capture the entirety of the F I emission.

3.3 Qualitative comparison of spectra obtained at atmospheric and reduced ablation atmosphere pressure

Until now, changes to intensity related to a variation of ablation atmosphere pressure were assessed with a PI film standard containing sufficient F to distinguish the F I emission peak from the background. To demonstrate that the systematic improvement with pressure reduction applies to other concentrations and possibly also to other matrices, a standard with a F concentration of 356 μg g^{-1} as well as the NIST SRM610 were measured with the acquisition parameters determined by the parameter optimization.

The NIST SRM610 is a glass reference material commonly applied in laser-ablation-based techniques and while it does not contain a certified mass fraction of F, several works have measured its F content. The GeoReM database for reference materials and isotopic standards of geochemical and mineralogical interest[38,39] provides a preferred value for the F concentration of 304 μg g^{-1} in NIST SRM610 and in the most recent work listed by the GeoReM database, Kendrick *et al.*[40] determined a F concentration of 287 ± 16 μg g^{-1}. Hence, the PI standard used for comparison in this section was chosen as it contains a similar nominal F concentration.

Fig. 6 depicts the spectra obtained from analyzing the PI standard at reduced and atmospheric pressure. The spectra in Fig. 6a and c are comparable, though the noise within the spectrum is diminished at reduced pressure. Moreover, in the zoomed-in regions in Fig. 6c and d, a notable increase in the intensity at approx. 685.65 nm can be observed at reduced pressure, corresponding to the F I emission. Regardless of pressure, a shoulder to the right of the F I emission is visible, which will be addressed further in the following sections.

Spectra acquired from NIST SRM610 with the same experimental settings are illustrated in Fig. 7. What is immediately

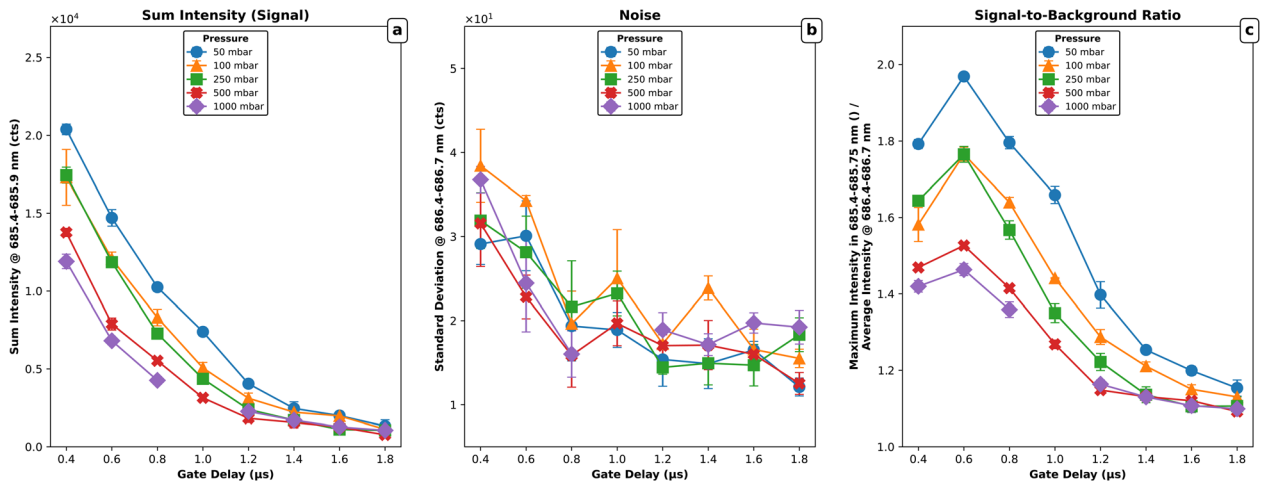

Fig. 5 Comparison of metrics for different ablation atmosphere pressures and gate delays. (a) Sum intensity around the most intense F I emission line in the investigated spectral range (685.4–685.9 nm, local background subtraction). (b) Noise, determined as the standard deviation in a region of 686.4–686.7 nm. (c) Signal-to-background ratio, calculated by dividing the maximum within 685.4–685.75 nm by the average intensity within 686.4–686.7 nm. Spectra used for evaluation (see SI Fig. S4) resemble the average of 42 shots from the analysis of a standard containing 2145 μg g^{-1} F, acquired with a laser energy of 8.21 mJ and a gate width of 0.5 μs. Error bars represent the standard deviation of five repeat measurements.

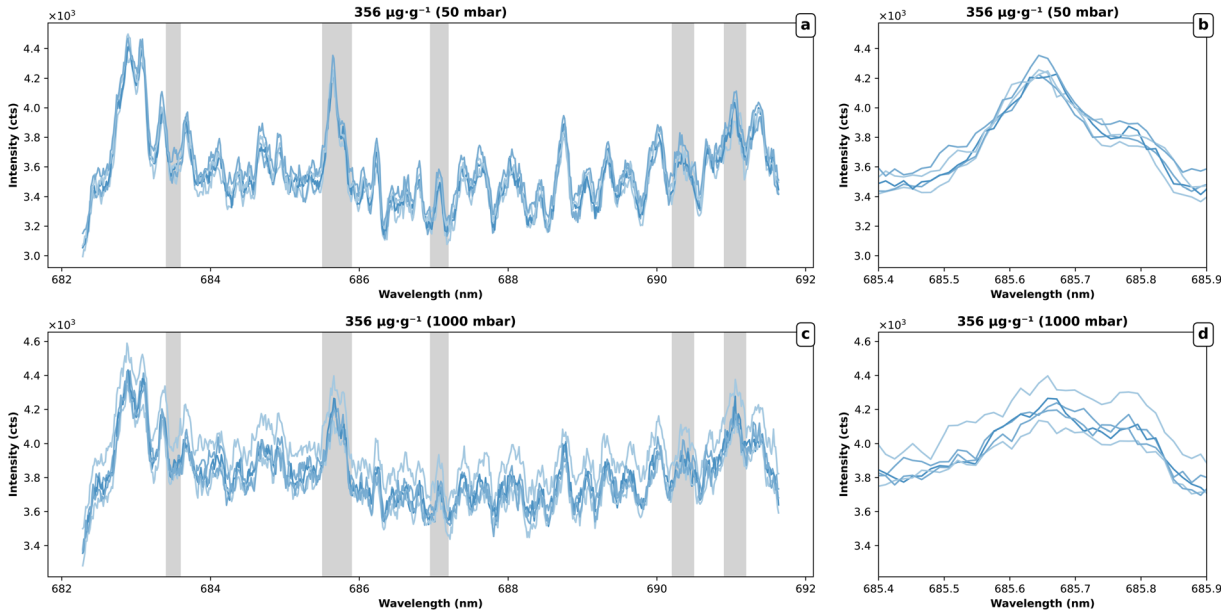

Fig. 6 Spectra (five repeat measurements) obtained from a PI standard with 356 µg g^{-1} added F at (a) and (b) atmospheric and (c) and (d) reduced ablation atmosphere pressure. (a) and (c) show the full spectra, whereas (b) and (d) focus on the region with the most intense F I emission in the measured range marked by the shaded area at ~685.7 nm in (a) and (c), respectively. Spectra represent the average of 82 shots acquired with a laser energy of 8.21 mJ, a gate delay of 0.4 µs and a gate width of 2.0 µs.

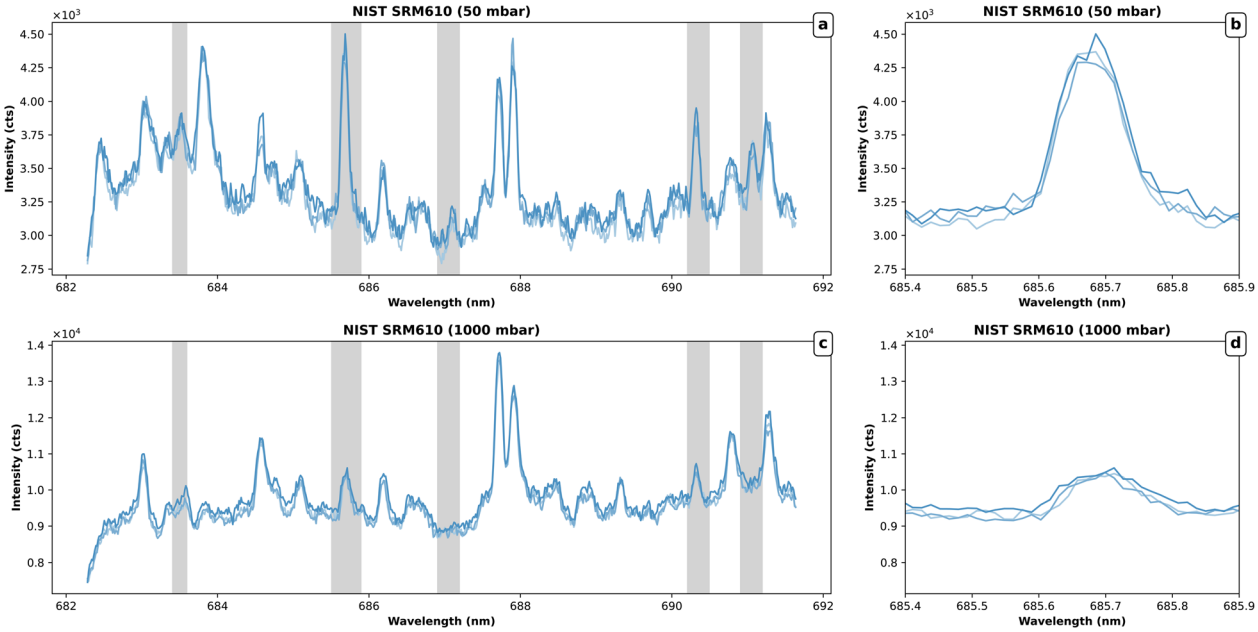

Fig. 7 Spectra (three repeat measurements) obtained from the NIST SRM610 at (a) and (b) atmospheric and (c) and (d) reduced ablation atmosphere pressure. (a) and (c) show the full spectra, whereas (b) and (d) focus on the region with the most intense F I emission in the measured range marked by the shaded area at ~685.7 nm in (a) and (c), respectively. Spectra represent the average of 42 shots acquired with a laser energy of 8.21 mJ, a gate delay of 0.4 µs and a gate width of 2.0 µs.

clear when contrasting Fig. 6 and 7, is that the aforementioned shoulder to right of the F I emission is not observable for the glass standard, supporting the claim that the shoulder is pertinent to polymers. Moreover, the spectra indicate that the enhancement is more pronounced for the NIST SRM610 compared to the polyimide standard with a similar concentration, while the background is smoother. The general trends due to pressure reduction, *i.e.*, noise reduction and increased intensity of the F I emission, apply in the same manner as for the PI standard. Hence, it can be assumed that the enhancement for F at reduced pressure may also be observed for glass matrices. Interestingly, the intensity of

several other peaks, which could not be assigned to elements with certainty, are also affected by the pressure change to different extents.

3.4 Univariate calibration: choice of normalization and background subtraction approaches

In order to perform quantification of F in PI, calibrations were performed at reduced and atmospheric ablation atmosphere pressure with a set of polyimide-based standards, which contained between 0 and 2145 μg g^{-1} added F. For the comparison of the calibration performance, it was important to find suitable data processing steps for both background subtraction and normalization.

Fig. 8 compares spectra obtained from the measurement of the polyimide standards at atmospheric and reduced pressure (50 mbar). From the full wavelength range in Fig. 8a and d it is clear that the peak intensity of the most intense F I emission (~685.7 nm) increases with concentration. Additionally, when contrasting the two ablation atmosphere pressures, the enhancement for F can be observed. This is especially visible for the less intense F I emissions in the measured wavelength range (grey shaded areas in Fig. 8a and d), which at atmospheric pressure are barely distinguishable from the highly structured background even at higher concentrations.

Looking at a narrower wavelength range around the F I emission at ~685.7 nm in Fig. 8b and e, a difference in absolute intensity of the background can be observed, indicating the need for background subtraction. Moreover, a shoulder to the right of the F I emission can be seen whose intensity does not seem to change with F concentration. This suggests that some deconvolution of the two peaks, one corresponding to the F I emission and the other to the shoulder, should be performed to determine whether it affects calibration performance.

Furthermore, applying normalization to the spectra is a common step in LIBS literature to equalize differences between replicate measurements of the same sample or different samples. As Guezenoc, Gallet-Budynek, and Bousquet discussed in their review on normalization approaches for quantitative LIBS analyses,[41] there is no universally applicable and accepted spectra normalization method, contrary to other spectroscopic techniques such as Near-Infrared Spectroscopy or Inductively Coupled Plasma-Atomic Emission Spectroscopy. Moreover, they refer to a work of Tognoni and Cristoforetti,[42] who compared three different normalization procedures and ultimately concluded that the appropriate strategy was dependent on the experiment context.

In this work, we decided on three different approaches to calculate values as input for univariate regressions:

- Non-normalized (NN): sum intensity within 685.4–685.9 nm after background subtraction of a local linear background, which was calculated as a linear function from the average intensity within 685.15–685.25 and within 685.95–686.05 nm.
- Signal-to-background ratio (SBR): maximum intensity within 685.4–685.75 nm (reduced upper limit to avoid the background shoulder) divided by the average intensity within 686.4–686.7 nm – a featureless area of moderately constant intensity (*cf.* Section 3.1 and Fig. 2).
- Pseudo-Voigt fitting + deconvolution (PVD): deconvolution of the F I emission and background shoulder by fitting two pseudo-Voigt fits to the spectra, preceded by local linear background subtraction.

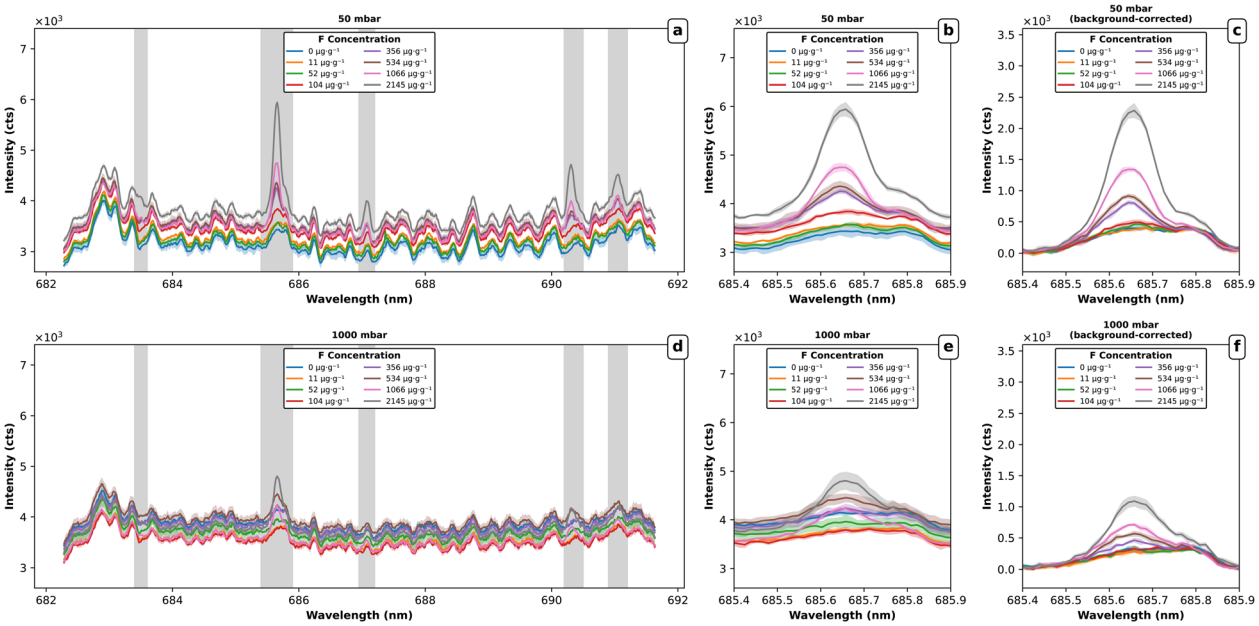

Fig. 8 Spectra comparison of the calibration standards at (a)–(c) 50 mbar and (d)–(f) at atmospheric pressure. (a) and (d) Illustrate the full spectra, whereas (b) and (e) show the zoomed-in wavelength range for the F I emission at ~685.7 nm; (c) and (f) depict the background-corrected spectra in that range. Each replicate measurement resulted in an average spectrum of 82 shots acquired with a laser energy of 8.21 mJ, a gate delay of 0.4 μs and a gate width of 2.0 μs. The mean spectrum of the five replicates is plotted here, with the surrounding shaded area representing the standard deviation.

The detailed reasoning for these choices can be found in SI Section S6. A description of the deconvolution approach is given in SI Section S7. Fig. 8c and f demonstrate the performance of the local linear background subtraction, showing that the background could be fitted appropriately. It is important to note that these methods were chosen as a result of the context of the investigation. This includes factors like the samples themselves (polymers/polyimides led to structured background), the detection system (detection unit with narrow spectral range), and the need for comparability between different ablation atmosphere pressures.

3.5 Univariate calibration: comparison of different metrics and their performance

In order to demonstrate the systematic improvement of sensitivity with a reduction of ablation atmosphere pressure, univariate calibration models were constructed for the three metrics highlighted at the end of Section 3.4 based on the spectra obtained from five repeat measurements on a set of 8 polyimide-based standards. The acquisition parameters employed for these measurements were as follows: 8.21 mJ laser energy; 0.4 μs gate delay; 2.0 μs gate width. For the calibration experiments and the subsequent sample measurements, the spectra of 82 laser shots were averaged. These parameters were kept the same for comparison between reduced and atmospheric pressure. Scott, Effenberger, and Hatch[7] note that this may not be appropriate for the combination of gate width and gate delay. However, as can be deduced from Section 3.2, we found that the main difference in the spectra with the same gate delay (larger than 0.4 μs) at different pressures was the signal-to-background ratio.

To evaluate and compare the performance of the univariate calibrations, the intercept, slope, coefficient of determination (R^2), root mean square error or calibration (RMSE), root mean square error of cross-validation (RMSECV, using Leave-One-(Standard-)Out as cross validation method) and limit of detection (LOD) were calculated for the linear regression of the processed data. For the linear regressions, the mean value of the five replicate measurements entered the regression and the reciprocals of the squared standard deviation were used as weights.

The LOD is a performance metric that must be examined and defined more precisely. In the context of analytical chemistry, the LOD is typically calculated from the expression corresponding to the definition of the LOD by IUPAC.[43] However, other definitions of the LOD have been discussed and applied in the field. We attempted to compare four different approaches in SI Section S8 (including the mathematical equation when applicable), which are summarized as follows:

- The IUPAC accepted definition using the standard deviation of the blank; refers to eqn (1) with $k = 3$; denoted $\mathrm{LOD}^{\mathrm{blank}}$.
- The rearranged expression suggested by Hahn and Omenetto[43] that utilizes the signal of a standard with known concentration; refers to eqn (4) with $k = 3$ and using the average signal of the standard with the highest concentration (2145 μg g^{-1} F); denoted $\mathrm{LOD}^{\mathrm{max}}$.
- The equation which replaces the standard deviation of the blank with the standard error of the intercept; refers to eqn (5) with $k = 3$; denoted $\mathrm{LOD}^{\mathrm{intercept}}$.
- The definition by Hubaux and Vos,[44] evaluated graphically by determining the intersection point of a horizontal line at the decision limit with the lower confidence band of the regression curve; denoted $\mathrm{LOD}^{\mathrm{H–V}}$.

We assess these four definitions of the LOD to investigate changes in calibration performance for different evaluation metrics and ablation atmosphere pressures. The above list is not complete; other approaches are possible and applied in LIBS literature. In fact, one of the most common approaches is to assume that the standard deviation of the background intensity is indicative of the measurement error, thereby replacing the standard deviation of the blank in eqn (S1), for example. While this is a reasonable approach, particularly when no analytical blank is available (which is often the case for LIBS), many authors fail to elaborate on what the background exactly is (*e.g.*, omitting the wavelength range) and how many data points are used for calculation of the standard deviation. We are in the fortunate situation where it can be assumed that the calibration standard without added F can be taken – if not as an analytical blank – as a procedural blank standard.

Table 1 gives an overview of the performance of the univariate calibration models at reduced and atmospheric pressure and for the previously discussed evaluation metrics. The corresponding calibration curves are depicted in SI Fig. S6–S8. For the slope, *i.e.*, the sensitivity, all evaluation metrics show a similar trend, namely an increase with reduced pressure. At 50 mbar ablation atmosphere pressure, the sensitivity is roughly twice as large as at atmospheric pressure. The linearity (R^2) is generally high for all metrics and both pressures, but is augmented at reduced pressure.

Looking at the values for the different definitions of the LOD, it becomes clear why a strong focus of this work was to compare the approaches. On the one hand, it is apparent that the LOD is markedly reduced by a pressure reduction for all methods, with relative deviations ranging from ~50 to ~80% when comparing 50 mbar to atmospheric pressure. On the other hand, there is a large disparity between the LOD definitions. Overall, the lowest values are returned when using the standard error of the intercept as estimate, *i.e.*, $\mathrm{LOD}^{\mathrm{intercept}}$, with a notable exception being the $\mathrm{LOD}^{\mathrm{max}}$ when evaluating the SBR. The Hubaux–Vos method expectedly delivers the highest values for the LOD, but still exhibits the same downward trend with pressure. From the perspective of different evaluation metrics, the SBR approach outperforms both the NN and PVD metrics.

The values given in Table 1 would suggest that concentrations as low as 13 μg g^{-1} can be detected by evaluating the SBR at a pressure of 50 mbar, which is significantly lower than reported for the atomic F I emission in most literature and also undercuts many works using the molecular emission, where the augmented emission by a molecular species (usually CaF) is detected. For instance, Quarles *et al.*[10] reported a LOD of 135 μg g^{-1} in geological samples and Pořízka *et al.*[15] a value of 150 μg g^{-1} using pressed powder standards for the atomic emission. In the same work, Pořízka *et al.* determined a LOD of 65 μg g^{-1}

Table 1 Performance comparison of univariate calibration models for different evaluation metrics and ablation atmosphere pressures. Linear regressions were weighted by the inverse square of the standard deviation of repeat measurements ($n = 5$). Values were rounded to three significant digits[a]

Metric	Pressure (mbar)	Slope (a.u. g μg^{-1})	Intercept (a.u.)	R^2 ( )	RMSE (μg g^{-1})	RMSECV (μg g^{-1})	LOD^{blank} (μg g^{-1})	LOD^{max} (μg g^{-1})	LOD^{intercept} (μg g^{-1})	LOD^{H-V} (μg g^{-1})
NN	50	8.82×10^{0}	8.67×10^{3}	0.999	14	25	93	63	29	104
	1000	4.32×10^{0}	6.78×10^{3}	0.970	70	93	311	179	107	505
SBR	50	2.47×10^{-4}	1.16×10^{0}	0.989	29	38	40	13	39	80
	1000	1.00×10^{-4}	1.12×10^{0}	0.981	54	77	114	18	72	192
PVD	50	1.51×10^{-1}	7.55×10^{1}	0.996	22	39	46	39	30	55
	1000	0.85×10^{-1}	7.08×10^{1}	0.971	60	94	223	173	86	352

[a] NN = sum intensity within 685.4–685.9 nm after local linear background subtraction; SBR = signal-to-background ratio comparing the maximum intensity within 685.4–685.75 nm (signal) against the average intensity within 686.4–686.7 nm (background); PVD = amplitude of pseudo-Voigt profile attributed to the F emission after deconvolution of background-subtracted spectra; R^2 = coefficient of determination; RMSE = root mean square error of calibration; RMSECV = root mean square error of cross validation (using Leave-One-Out cross validation); see Section S8 of the SI for the different definitions of the LOD.

using the CaF emission. Furthermore, Alvarez-Llamas, Pisonero, and Bordel[16] state a LOD of 49 μg g^{-1} and in a recent study by Quarles *et al.*[14] the LOD was found to be as low as 4 μg g^{-1} when detecting the molecular emission. Especially when considering the raw and/or background-corrected spectra of the calibration standards (see Fig. 8), we leave it up to the reader to decide the validity of the calculated value reported here.

3.6 Multivariate calibration with partial least squares

Continuing on from the suggestion by Dyar *et al.*[45] that multivariate techniques could make spectral preprocessing (specifically baseline removal) redundant, it seems appropriate to investigate it for this topic. In fact, Quarles *et al.* previously evaluated the use of partial least squares (PLS) regression for the analysis of F and compared it to univariate methods, concluding that the multivariate method was more robust.[10] However, PLS has also been employed in several other contexts (*cf.*, for example,[46–48]).

In this work, a simplistic approach to PLS is taken, meaning that (parts of) the entire spectral range are directly fed to the PLS algorithm, implemented in Python *via* the scikit-learn package[49] (and more specifically the PLSRegression class in version 1.8.0). The only distinction made here is the difference between a full spectrum, *i.e.*, using the entire spectrum, and a sparse spectrum with the idea to reduce the noise that enters the PLS algorithm. Compared to the full spectrum approach, the sparse model only considers wavelength ranges corresponding to the F I emission in the measured spectral range, namely: (683.2, 683.8), (685.3–686.0), (686.8, 687.3), (690.0, 690.6), and (690.8, 691.3). Furthermore, the C I emission was also considered by including the range (682.7–683.1). A comparison between the full spectrum and the selected wavelength ranges can be found in SI Fig. S11.

Out of the box, scikit-learn's PLSRegression applies standardization to both the input spectra and concentration when used in the context of calibration. In contrast to the univariate calibration model, which used the mean value from repeat measurements (and the standard deviation as error), the PLS models were built on the spectra of all repeat measurements. The number of latent variables was determined by performing cross-validation based on scikit-learn's GroupKFold to ensure that all repeat measurements of one standard were removed during the cross-validation step. The results are shown in SI Fig. S9, but the key takeaway is that three latent variables were chosen for all pressures and for both the full and sparse models. When looking at the loadings of these latent variables (see SI Fig. S10 for atmospheric pressure), one can interpret the second latent variable as the reconstruction of the F I emission in the observed spectral range and the third latent variable as the general noise of the spectra.

While quantities like the RMSE, RMSECV, and R^2 can easily be obtained from the PLS model, the LOD is not as straightforward. In this regard, we refer to Allegrini and Oliveira who discussed an approach specifically for PLS that follows IUPAC definitions, whereby it is customary to provide a range for the LOD.[50] If the predicted concentration is below the lower value, LOD_{min}, no analyte is detected. If the predicted concentration is above the upper value, LOD_{max}, analyte is present. A further difference compared to univariate models is the definition of the sensitivity, SEN, which for PLS is the reciprocal of the Euclidian norm of the regression vector, *i.e.*, the vector of regression coefficients.

Table 2 provides an overview of the performance metrics of the full and sparse spectrum PLS models for the different ablation atmosphere pressures. Plots comparing the reference and predicted concentration are illustrated in SI Fig. S11. Despite the full spectrum model generally exhibiting lower linearity and the RMSECV being markedly higher than the sparse model, the corresponding LOD ranges are lower. On the contrary, the sensitivity is higher for the full spectrum model, most likely leading to the improved LOD. In any case, the trend of improved sensitivity with reduced ablation atmosphere pressure can be observed for multivariate analysis too, reducing the LOD by approx. 50%. The LODs of the PLS models are in a comparable range as those of the univariate calibration models, performing somewhat similar to the LOD^{H-V}.

3.7 Quantification of F in polyimide samples

The univariate and multivariate models discussed in Sections 3.5 and 3.6, respectively, were applied to 7 polyimide-based

Table 2 Performance comparison of the full and sparse spectrum PLS models at different ablation atmosphere pressures. PLS models were constructed based on five repeat measurements of 8 calibration standards. Values were rounded to three significant digits. *Cf.*[50] for interpretation of the LOD values[a]

Method	Pressure (mbar)	SEN (a.u. g μg^{-1})	R^2 ( )	RMSE (μg g^{-1})	RMSECV (μg g^{-1})	LOD_{min} (μg g^{-1})	LOD_{max} (μg g^{-1})
Full spectrum	50	1.82	0.968	32	124	115	121
	1000	1.03	0.845	51	274	265	286
Sparse	50	1.37	0.987	20	81	156	168
spectrum	1000	0.89	0.894	63	226	317	338

[a] SEN = sensitivity of the PLS model, given by the inverse of the length of the regression coefficients; R^2 = coefficient of determination; RMSE = root mean square error of calibration; RMSECV = root mean square error of cross validation (using Leave-One-Standard-Out cross validation); LOD_{min} = lower limit of the LOD range; LOD_{max} = upper limit of the LOD range.

samples with unknown concentration, denoted PI 1 through PI 7. The exact polymer structure of the samples is unknown, but following on from the comparison of the background of different polymers (see SI Section S2), it can be assumed that the degree of matrix matching between standards and samples is high. An overview of the spectra of the samples at 50 and 1000 mbar ablation atmosphere pressure (with focus on the F I emission and after background subtraction) is given in SI Fig. S12. For the samples PI 2, 3, 4, and 5, no significant signal above that of a blank standard is visible at atmospheric pressure and the shoulder to the right of the F I emission dominates the spectra. This changes for 50 mbar, where only PI 3 remains almost identical to the blank standard.

Hence, it can already be predicted that the concentration of some samples will fall below the LOD or even deliver negative results, especially for atmospheric pressure. Table 3 summarizes the determined concentration by plainly inserting the values into the univariate models based on the evaluation metrics introduced in Section 3.4. Bar charts for the different metrics and pressures that compare the concentrations to the intercept and LOD^{H-V} can be found in Section S13 of the SI. The aforementioned prediction holds true for all approaches, though there are some differences when comparing values of the two pressures. There is no clear trend between the metrics as to which samples are systematically over- or underestimated. For instance, PI 7 is predicted to have a markedly higher concentration by the reduced pressure calibration for the NN and PVD method, but not for the SBR. Conversely, PI 6 has a comparable predicted concentration for all metrics and for both pressures. Surprisingly, there is only one metric that results in a positive concentration for all investigated samples at reduced pressure, namely the PVD approach, where only PI 3 is estimated to have a concentration below LOD^{H-V}.

Additionally, Table 3 summarizes the concentrations predicted for the samples by the full and sparse spectrum PLS models at 50 and 1000 mbar. Bar charts that compare the concentrations to the LOD range for the full and sparse model and the two pressures are depicted in SI Fig. S16. The concentration of the samples is consistently predicted to be below zero at atmospheric pressure for both the sparse and full spectrum method (except for PI 7 for the latter). This is somewhat surprising as the results for the univariate models would indicate that some of the sample concentrations are in a region that is above the LOD range (317–338 μg g^{-1} and 265–286 μg g^{-1} for the sparse and full spectrum model, respectively). Then again, when looking at the sample spectra at atmospheric pressure (SI Fig. S12), it can be appreciated that the models predict low or even negative concentrations. For 50 mbar, the full spectrum model predicts positive concentrations for all samples (with PI 2, 3, and 4 estimated to be below the LOD range), whereas the sparse spectrum model predicts four samples to be below the LOD range, with PI 2, 3, and 4 predicted to have negative concentration. This, combined with the generally higher sensitivity of the full spectra models, would indicate that the full spectrum contains more information relevant to the calibration than the regions selected for the sparse models.

3.8 So what exactly is the limit of detection of fluorine in polyimide?

Seeing that there is a variation between the LOD values within the univariate models, between the PLS models, and comparing all models presented in this work for a specific ablation atmosphere pressure, it is reasonable to pose the question, what value for the LOD is actually viable for the determination of F in PI. This matter is somewhat subjective, because from an analysts standpoint any one method which results in a lower LOD (or, in extension, limit of quantification) and higher sensitivity will generally be favoured. However, we hope that from the above discussion it is clear that a calculated value for the LOD does not necessarily indicate that the spectra from a sample containing a concentration slightly above the LOD can be distinguished from a blank sample. All in all, it can be concluded that an evaluation metric that reduces the LOD can always be constructed, but this metric must be assessed in relation to the raw spectra, especially those of a blank standard (if available).

Similarly, the definition of the LOD may be chosen to achieve the lowest achievable value without assessing whether this actually constitutes an observable difference between the spectra of a blank standard and a standard with concentration slightly above the LOD. Both LOD^{max}, which basically extrapolates the value of a standard with high concentration to zero concentration, and $LOD^{intercept}$, whose absolute value is closely

Table 3 F concentration in the unknown samples, evaluated with different metrics and at different ablation atmosphere pressures using univariate and PLS calibration models. Values were rounded to three significant digits. For the univariate models, values below the Hubaux–Vos LOD are denoted with LOD^{H-V}; for the multivariate models, values below the upper limit of the LOD range are denoted with LOD_{max}; negative values are additionally marked with ●. The error indicated here is the standard deviation of five repeat measurements[a]

			Concentration (μg g^{-1})						
Metric	Pressure (mbar)	LOD (μg g^{-1})	PI 1	PI 2	PI 3	PI 4	PI 5	PI 6	PI 7
NN	50	104	269 ± 87	110 ± 71	<LOD^{H-V}●	<LOD^{H-V}	230 ± 43	426 ± 41	834 ± 52
	1000	505	<LOD^{H-V}	<LOD^{H-V}	<LOD^{H-V}●	<LOD^{H-V}●	<LOD^{H-V}	<LOD^{H-V}	519 ± 105
SBR	50	80	169 ± 41	<LOD^{H-V}●	<LOD^{H-V}●	<LOD^{H-V}●	<LOD^{H-V}●	444 ± 44	620 ± 35
	1000	192	68 ± 36	<LOD^{H-V}●	<LOD^{H-V}●	<LOD^{H-V}●	<LOD^{H-V}●	352 ± 122	510 ± 105
PVD	50	55	346 ± 43	154 ± 39	<LOD^{H-V}	121 ± 32	285 ± 20	494 ± 34	866 ± 24
	1000	352	<LOD^{H-V}	<LOD^{H-V}	<LOD^{H-V}●	<LOD^{H-V}●	<LOD^{H-V}	456 ± 55	574 ± 39
Full	50	121	210 ± 21	<LOD_{max}	<LOD_{max}	<LOD_{max}	423 ± 43	297 ± 47	692 ± 40
PLS	1000	286	<LOD_{max}●	<LOD_{max}●	<LOD_{max}●	<LOD_{max}●	<LOD_{max}●	<LOD_{max}●	<LOD_{max}
Sparse	50	168	<LOD_{max}	<LOD_{max}●	<LOD_{max}	<LOD_{max}●	215 ± 32	182 ± 42	586 ± 44
PLS	1000	338	<LOD_{max}●	<LOD_{max}●	<LOD_{max}●	<LOD_{max}●	<LOD_{max}●	<LOD_{max}●	<LOD_{max}●

[a] NN = sum intensity within 685.4–685.9 nm after local linear background subtraction; SBR = signal-to-background ratio comparing the maximum intensity within 685.4–685.75 nm (signal) against the average intensity within 686.4–686.7 nm (background); PVD = amplitude of pseudo-Voigt profile attributed to the F emission after deconvolution of background-subtracted spectra; full PLS = PLS performed on the full wavelength range; sparse PLS = PLS performed on selected wavelength regions; LOD = Limit of Detection (determined with the Hubaux–Vos method for univariate models and equal to the upper limit of the LOD range for multivariate models).

tied to the width of the confidence band at zero concentration, consistently returned lower values than LOD^{blank}. However, a sample with the concentration of the LOD^{max} obtained for the SBR at 50 mbar (13 μg g^{-1}) almost certainly cannot be discerned from a blank standard, judging from the raw spectra of the calibration standards. Hence, it is of utmost importance to compare the value obtained for the LOD to the experimentally measured spectra, *i.e.*, analyzing calibration standards close to the LOD.

In that sense, evaluating the LOD^{H-V} for the univariate models seemed to result in concentrations, at which spectra could also visually be differentiated from those of a blank standard. The returned values are generally higher than the other definitions, but are much more representative of actually observable signal differences. In that regard, the LOD was reduced from 505 μg g^{-1} to 104 μg g^{-1} (non-normalized sum intensity), 192 μg g^{-1} to 80 μg g^{-1} (SBR), and 352 μg g^{-1} to 55 μg g^{-1} (pseudo-Voigt fitting + deconvolution) comparing atmospheric pressure to 50 mbar employing the respective evaluation metrics.

Furthermore, it is important to note that the multivariate models significantly underestimated the concentrations of the samples at atmospheric pressure compared to the univariate models. Only at reduced pressure, where the signal-to-background ratio was drastically improved for the samples, the calculated concentrations where in a similar range to those of the univariate models. Overall, the full spectrum approach achieved better sensitivity and LODs; pressure reduction resulted in a decrease of the LOD range from 265–286 μg g^{-1} to 115–121 μg g^{-1} when comparing atmospheric pressure and 50 mbar. These values are comparable to the LOD^{H-V} of the univariate models, which reaffirms that it is the most appropriate LOD definition for the univariate models.

All things considered, we suggest that the non-normalized sum intensity is the most sensible evaluation metric for univariate calibration models and that the LOD is assessed as defined by Hubaux and Vos. Hence, the LOD could be improved by ~80% from 505 μg g^{-1} to 104 μg g^{-1} when reducing the ablation atmosphere pressure from 1000 mbar to 50 mbar. For the multivariate models the full spectrum PLS generally exhibited higher sensitivity and reduced LOD ranges. The LOD was lowered from 265–286 μg g^{-1} at atmospheric pressure to 115–121 μg g^{-1} at 50 mbar, representing a relative improvement of ~40%.

These values are comparable to literature using molecular LIBS based on the CaF emission (*cf.*, *e.g.*, ref. 15 and 16), but the approach employing reduced pressure could provide some significant benefits. Initial works on CaF by, *e.g.*, Gaft *et al.*[12] and Alvarez-Llamas, Pisonero, and Bordel[11] focused on Ca-containing samples, thereby requiring Ca to be present in sufficient quantities in the matrix. In a follow-up study Alvarez-Llamas, Pisonero, and Bordel[16] demonstrated a nebulization approach for Ca-free samples. Méndez-López *et al.*[51,52] also showed that the approach is applicable when the nebulized liquid is the investigated sample. The main difficulty with nebulization is the susceptibility to formation of liquid islands on top of the sample, which inherently limits the spatial resolution on the surface and especially with regards to depth. Weiss *et al.*[17] discussed the possibility of elemental mapping of F *via* the molecular CaF or CuF emission by either depositing calcium acetate or sputtering a thin Cu layer on the sample surface, respectively. They were able to perform imaging, but since ablation parameters were adjusted such that the surface layer was ablated completely, depth resolution cannot be achieved this way. It can be assumed that the spatial resolution (both in depth and at the surface) is not affected by a reduction of ablation atmosphere pressure, making the approach a useful alternative.

It should be pointed out that due to the lack of certified reference materials for a polyimide matrix, an assessment of the

trueness and therefore the accuracy of the method was not carried out. In fact, while certified reference materials for targeted PFAS analysis as well as for total fluorine content determination in other matrices (*e.g.*, BCR-461 for F in clay) exist, no equivalent for the total fluorine content in polymer matrices exists to the best of our knowledge. Therefore, it is difficult to decide which evaluation metric is the most applicable. However, it is clear that the performance suggested by the SBR does not transfer to an observable difference in the spectra. Looking at the PVD approach, it is also conceivable that the fitting routine performs worse at lower concentrations, where the amplitude of the analyte peak may be overestimated.

4. Conclusion

A detailed study of the quantification of F in polyimide and the impact of the ablation atmosphere pressure on the F signal was conducted. The initial parameter optimization regarding the laser energy and gate delay at different ablation atmosphere pressures showed that the signal intensity and the SBR of the F I emission at ~685.7 nm could be improved significantly by reducing the pressure. An increase in laser energy lead to a boost in intensity, which could be attributed to higher ablation rates, though it was evident that a reduction of pressure further improved signal intensity even at lower pulse energies. The found optimum gate delay of approx. 0.4 μs was in agreement with previous literature. Interestingly, this optimal gate delay was the same for all ablation atmosphere pressures, though the signal-to-background ratio was markedly enhanced at reduced pressure.

Three different evaluation metrics for univariate calibration models were discussed and their performance compared for reduced and atmospheric pressure. Furthermore, four distinct definitions of the LOD were investigated to assess the meaningfulness of this metric in the context of this investigation. Generally, a reduction in pressure yielded higher sensitivity (based on the slope of weighted linear regressions), regardless of the evaluation approach, but did not necessarily deliver lower LODs. Even though the calculated LOD values (as low as 13 μg g^{-1} for the SBR at 50 mbar) would indicate remarkable improvements with reduced ablation atmosphere pressure for the F I emission compared to literature, spectra that correspond to a standard with a concentration in the vicinity of the LOD were not discernible from those of a blank standard. The most representative value was determined to be the non-normalized sum intensity in combination with Hubaux–Vos definition, yielding a LOD of 505 μg g^{-1} at atmospheric pressure and 104 μg g^{-1} at 50 mbar for univariate regression. The LOD range of the multivariate PLS regression model using the full spectrum as input was improved from 265–286 μg g^{-1} to 115–121 μg g^{-1} when comparing atmospheric pressure and 50 mbar.

Overall, this investigation highlights and reemphasizes the importance of performing calibration at concentrations close to the reported LOD in atomic spectroscopy. As pointed out by, *e.g.*, Neubauer,[53] calibrations curves obtained from high-concentration standards can impair the representativeness of the calculated LOD value, especially if low-concentration samples are supposed to be measured. In this work, we found that the main limitation for the analysis of F in polyimide was the highly structured background that seems to arise from polymer analysis in general within the measured spectral range. In essence, the compromised overall method performance due to this background can be interpreted as a matrix effect, which stems from the polymer matrix.

Regardless, the reduced ablation atmosphere pressure method holds promise for the determination of other non-metals with generally mediocre sensitivity in LIBS, *e.g.*, Cl, Br, O, and N. Furthermore, the approach could serve as an alternative to molecular LIBS. Even though sensitivity using molecular CaF emission may achieve slightly better sensitivity (*cf.* Quarles *et al.* with a LOD of 4 μg g^{-1} (ref. 14)), the approach demonstrated here imposes less restrictions on the sample and leverages the spatial resolution of the LIBS setup employed, making spatially resolved measurements possible also in Ca-free samples.

Author contributions

David Ken Gibbs: conceptualization, data curation, formal analysis, investigation, methodology, software, validation, visualization, writing – original draft, writing – review & editing. Andreas Limbeck: conceptualization, formal analysis, funding acquisition, project administration, resources, supervision, writing – review & editing.

Conflicts of interest

There are no conflicts to declare.

Data availability

The data supporting the findings of this study are available within the article or its supplementary information (SI). Other relevant data can be shared upon reasonable request. Supplementary information is available. See DOI: https://doi.org/10.1039/d6ja00144k.

Acknowledgements

This work was funded by the Austrian Federal Ministry of Labour and Economy, the National Foundation for Research, Technology and Development and the Christian Doppler Research Association is gratefully acknowledged (Christian Doppler Laboratory "Multiscale Chemical Analysis of Materials in Industrial Processing and Use"). The authors greatly acknowledge the TU Wien Bibliothek for financial support through its Open Access Funding Program. The authors would like to extend their gratitude to Patrick Tapler for the early investigations on fluorine quantification in polyimide and Luzie Kölling for the initial method development regarding the spin-coating process for the production of polyimide film standards. Moreover, the authors would like to thank Lukas Brunnbauer for the discussions on multivariate approaches.

References

1 European Chemicals Agency, *Background document to the Opinion on the Annex XV dossier proposing restrictions on per- and polyfluoroalkyl substances (PFAS)*, European Chemicals Agency, Helsinki, 2025, https://echa.europa.eu/documents/10162/cd583492-f5d4-e2e7-9938-a1d602084c72.

2 L. Schultes, G. F. Peaslee, J. D. Brockman, *et al.*, Total Fluorine Measurements in Food Packaging: How Do Current Methods Perform?, *Environ. Sci. Technol. Lett.*, 2019, **6**(2), 73–78, DOI: 10.1021/acs.estlett.8b00700.

3 L. R. R. Souza, Determination of Non-Metals by Molecular Absorption: A Minireview from the Beginning through Recent Developments in High-Resolution Continuum Source Molecular Absorption Spectrometry (HR-CS MAS), *Anal. Lett.*, 2021, **54**(16), 2574–2589, DOI: 10.1080/00032719.2021.1878526.

4 M. C. C. D. Ignacio, G. W. Curtzwiler, M. R. Early, *et al.*, Ion Selective Electrode (ISE) Method for Determination of Total Fluorine and Total Organic Fluorine in Packaging Substrates, *Methods Protoc.*, 2023, **6**, 10.

5 I. G. Idowu, O. D. Ekpe, D. Megson, *et al.*, A systematic review of methods for the analysis of total per- and polyfluoroalkyl substances (PFAS), *Sci. Total Environ.*, 2025, **967**, 178644, DOI: 10.1016/j.scitotenv.2025.178644.

6 M. P. Mateo, V. Piñon, D. Anglos, *et al.*, Effect of ambient conditions on ultraviolet femtosecond pulse laser induced breakdown spectra, *Spectrochim. Acta, Part B*, 2012, **74–75**, 18–23, DOI: 10.1016/j.sab.2012.06.031.

7 J. R. Scott, A. J. Effenberger and J. J. Hatch, Influence of Atmospheric Pressure and Composition on LIBS, in *Laser-Induced Breakdown Spectroscopy: Theory and Applications*, ed. Musazzi, S. and Perini, U., Springer Berlin Heidelberg, 2014, pp. 91–116.

8 M. Tran, B. W. Smith, D. W. Hahn, *et al.*, Detection of Gaseous and Particulate Fluorides by Laser-Induced Breakdown Spectroscopy, *Appl. Spectrosc.*, 2001, **55**(11), 1455–1461, DOI: 10.1366/0003702011953865.

9 D. A. Cremers and L. J. Radziemski, Detection of chlorine and fluorine in air by laser-induced breakdown spectrometry, *Anal. Chem.*, 1983, **55**(8), 1252–1256, DOI: 10.1021/ac00259a017.

10 C. D. Quarles, J. J. Gonzalez, L. J. East, *et al.*, Fluorine analysis using Laser Induced Breakdown Spectroscopy (LIBS), *J. Anal. At. Spectrom.*, 2014, **29**(7), 1238–1242, DOI: 10.1039/c4ja00061g.

11 C. Álvarez, J. Pisonero and N. Bordel, Quantification of fluorite mass-content in powdered ores using a Laser-Induced Breakdown Spectroscopy method based on the detection of minor elements and CaF molecular bands, *Spectrochim. Acta, Part B*, 2014, **100**, 123–128, DOI: 10.1016/j.sab.2014.07.024.

12 M. Gaft, L. Nagli, N. Eliezer, *et al.*, Elemental analysis of halogens using molecular emission by laser-induced breakdown spectroscopy in air, *Spectrochim. Acta, Part B*, 2014, **98**, 39–47, DOI: 10.1016/j.sab.2014.05.011.

13 C. Alvarez-Llamas, J. Pisonero and N. Bordel, Quantification of fluorine traces in solid samples using CaF molecular emission bands in atmospheric air Laser-Induced Breakdown Spectroscopy, *Spectrochim. Acta, Part B*, 2016, **123**, 157–162, DOI: 10.1016/j.sab.2016.08.006.

14 C. D. Quarles Jr, B. T. Manard, N. A. Zirakparvar, *et al.*, Exploration of a Combined LIBS and LA-ICP-MS Approach for Apatite Characterisation, *Geostand. Geoanal. Res.*, 2025, **50**(1), 67–83, DOI: 10.1111/ggr.70021.

15 P. Pořízka, S. Kaski, A. Hrdlička, *et al.*, Detection of fluorine using laser-induced breakdown spectroscopy and Raman spectroscopy, *J. Anal. At. Spectrom.*, 2017, **32**(10), 1966–1974, DOI: 10.1039/c7ja00200a.

16 C. Alvarez-Llamas, J. Pisonero and N. Bordel, A novel approach for quantitative LIBS fluorine analysis using CaF emission in calcium-free samples, *J. Anal. At. Spectrom.*, 2017, **32**(1), 162–166, DOI: 10.1039/c6ja00386a.

17 M. Weiss, Z. Gajarska, H. Lohninger, *et al.*, Elemental mapping of fluorine by means of molecular laser induced breakdown spectroscopy, *Anal. Chim. Acta*, 2022, **1195**, 339422, DOI: 10.1016/j.aca.2021.339422.

18 L. Brunnbauer, M. Jirku, C. D. Quarles Jr, *et al.*, Capabilities of simultaneous 193 nm - LIBS/LA-ICP-MS imaging for microplastics characterization, *Talanta*, 2024, **269**, 125500, DOI: 10.1016/j.talanta.2023.125500.

19 R. S. Harmon, R. E. Russo and R. R. Hark, Applications of laser-induced breakdown spectroscopy for geochemical and environmental analysis: A comprehensive review, *Spectrochim. Acta, Part B*, 2013, **87**, 11–26, DOI: 10.1016/j.sab.2013.05.017.

20 M. Bonta and A. Limbeck, Metal analysis in polymers using tandem LA-ICP-MS/LIBS: eliminating matrix effects using multivariate calibration, *J. Anal. At. Spectrom.*, 2018, **33**(10), 1631–1637, DOI: 10.1039/c8ja00161h.

21 J. A. Kreuz and J. R. Edman, Polyimide Films, *Adv. Mater.*, 1998, **10**(15), 1229–1232, DOI: 10.1002/(SICI)1521-4095(199810)10:15<1229::AID-ADMA1229>3.0.CO;2-B.

22 A. Sezer Hicyilmaz and A. Celik Bedeloglu, Applications of polyimide coatings: a review, *SN Appl. Sci.*, 2021, **3**(3), 363, DOI: 10.1007/s42452-021-04362-5.

23 H. Lei, S. D. Robert, J. L. Ralph, *et al.*, Mechanical properties of polyimide coated optical fibers at elevated temperatures, *Proc. SPIE*, 2016, **9702**, 97020Y, DOI: 10.1117/12.2210957.

24 M. Fahim, J. Bijwe and H. S. Nalwa, Chapter 8 – Polyimides for Microelectronics and Tribology Applications, in *Supramolecular Photosensitive and Electroactive Materials*, ed. Nalwa, H. S., Academic Press, 2001, pp. 643–726.

25 B. Achleitner, T. Huber, S. Larisegger, *et al.*, Monitoring the imidization reaction of polyimide thin films using an in-situ LIBS approach, *Polym. Test.*, 2024, **141**, 108647, DOI: 10.1016/j.polymertesting.2024.108647.

26 *NIST Atomic Spectra Database (ver. 5.12)*, https://physics.nist.gov/asd, accessed 25.01.2026.

27 Z. Gajarska, L. Brunnbauer and H. Lohninger, *et al.*, Advanced Polymer Characterization by LIBS, in *Laser-Induced Breakdown Spectroscopy in Biological, Forensic and*

Materials Sciences, ed. Galbács, G., Springer Nature Switzerland, 2025, pp. 413–442.
28 S. Trautner, J. Jasik, C. G. Parigger, *et al.*, Laser-induced optical breakdown spectroscopy of polymer materials based on evaluation of molecular emission bands, *Spectrochim. Acta, Part A*, 2017, **174**, 331–338, DOI: 10.1016/j.saa.2016.11.045.
29 I. Chamradová, P. Pořízka and J. Kaiser, Laser-Induced Breakdown Spectroscopy analysis of polymers in three different atmospheres, *Polym. Test.*, 2021, **96**, 107079, DOI: 10.1016/j.polymertesting.2021.107079.
30 Y. Iida, Effects of atmosphere on laser vaporization and excitation processes of solid samples, *Spectrochim. Acta, Part B*, 1990, **45**(12), 1353–1367, DOI: 10.1016/0584-8547(90)80188-O.
31 Ş. Yalçın, Y. Y. Tsui and R. Fedosejevs, Pressure dependence of emission intensity in femtosecond laser-induced breakdown spectroscopy, *J. Anal. At. Spectrom.*, 2004, **19**(10), 1295–1301, DOI: 10.1039/b404132a.
32 D. Wu, L. Sun, J. Liu, *et al.*, Parameter optimization of the spectral emission of laser-induced tungsten plasma for tokamak wall diagnosis at different pressures, *J. Anal. At. Spectrom.*, 2021, **36**(6), 1159–1169, DOI: 10.1039/d1ja00009h.
33 J. M. Vadillo, J. M. Fernández Romero, C. Rodríguez, *et al.*, Depth-resolved analysis by laser-induced breakdown spectrometry at reduced pressure, *Surf. Interface Anal.*, 1998, **26**(13), 995–1000, DOI: 10.1002/(SICI)1096-9918(199812)26:13<995::AID-SIA447>3.0.CO;2-D.
34 G. Galbács, Principle of Operation and Instrumentation for Laser-Induced Breakdown Spectroscopy, in *Laser-Induced Breakdown Spectroscopy in Biological, Forensic and Materials Sciences*, ed. Galbács, G., Springer Nature Switzerland, 2025, pp. 3–25.
35 C. K. Williamson, R. G. Daniel, K. L. McNesby, *et al.*, Laser-Induced Breakdown Spectroscopy for Real-Time Detection of Halon Alternative Agents, *Anal. Chem.*, 1998, **70**(6), 1186–1191, DOI: 10.1021/ac970362y.
36 M. A. Gondal, Y. W. Maganda, M. A. Dastageer, *et al.*, Detection of the level of fluoride in the commercially available toothpaste using laser induced breakdown spectroscopy with the marker atomic transition line of neutral fluorine at 731.1 nm, *Opt Laser. Technol.*, 2014, **57**, 32–38, DOI: 10.1016/j.optlastec.2013.09.035.
37 H.-Y. Moon, B. W. Smith and N. Omenetto, Temporal behavior of line-to-continuum ratios and ion fractions as a means of assessing thermodynamic equilibrium in laser-induced breakdown spectroscopy, *Chem. Phys.*, 2012, **398**, 221–227, DOI: 10.1016/j.chemphys.2011.07.002.
38 K. P. Jochum, U. Nohl, K. Herwig, *et al.*, GeoReM: A New Geochemical Database for Reference Materials and Isotopic Standards, *Geostand. Geoanal. Res.*, 2005, **29**(3), 333–338, DOI: 10.1111/j.1751-908X.2005.tb00904.x.
39 K. P. Jochum and U. Nohl, Reference materials in geochemistry and environmental research and the GeoReM database, *Chem. Geol.*, 2008, **253**(1), 50–53, DOI: 10.1016/j.chemgeo.2008.04.002.
40 M. A. Kendrick, J. D'Andres, P. Holden, *et al.*, Halogens (F, Cl, Br, I) in Thirteen USGS, GSJ and NIST International Rock and Glass Reference Materials, *Geostand. Geoanal. Res.*, 2018, **42**(4), 499–511, DOI: 10.1111/ggr.12229.
41 J. Guezenoc, A. Gallet-Budynek and B. Bousquet, Critical review and advices on spectral-based normalization methods for LIBS quantitative analysis, *Spectrochim. Acta, Part B*, 2019, **160**, 105688, DOI: 10.1016/j.sab.2019.105688.
42 E. Tognoni and G. Cristoforetti, [INVITED] Signal and noise in Laser Induced Breakdown Spectroscopy: An introductory review, *Opt Laser. Technol.*, 2016, **79**, 164–172, DOI: 10.1016/j.optlastec.2015.12.010.
43 D. W. Hahn and N. Omenetto, Laser-Induced Breakdown Spectroscopy (LIBS), Part II: Review of Instrumental and Methodological Approaches to Material Analysis and Applications to Different Fields, *Appl. Spectrosc.*, 2012, **66**(4), 347–419, DOI: 10.1366/11-06574.
44 A. Hubaux and G. Vos, Decision and detection limits for calibration curves, *Anal. Chem.*, 1970, **42**(8), 849–855, DOI: 10.1021/ac60290a013.
45 M. D. Dyar, S. Giguere, C. J. Carey, *et al.*, Comparison of baseline removal methods for laser-induced breakdown spectroscopy of geological samples, *Spectrochim. Acta, Part B*, 2016, **126**, 53–64, DOI: 10.1016/j.sab.2016.10.018.
46 V. C. Costa, M. L. de Mello, D. V. Babos, *et al.*, Calibration strategies for determination of Pb content in recycled polypropylene from car batteries using laser-induced breakdown spectroscopy (LIBS), *Microchem. J.*, 2020, **159**, 105558, DOI: 10.1016/j.microc.2020.105558.
47 S. M. Clegg, E. Sklute, M. D. Dyar, *et al.*, Multivariate analysis of remote laser-induced breakdown spectroscopy spectra using partial least squares, principal component analysis, and related techniques, *Spectrochim. Acta, Part B*, 2009, **64**(1), 79–88, DOI: 10.1016/j.sab.2008.10.045.
48 D. S. Ferreira, D. V. Babos, M. H. Lima-Filho, *et al.*, Laser-induced breakdown spectroscopy (LIBS): calibration challenges, combination with other techniques, and spectral analysis using data science, *J. Anal. At. Spectrom.*, 2024, **39**(12), 2949–2973, DOI: 10.1039/d4ja00250d.
49 F. Pedregosa, G. Varoquaux, A. Gramfort, *et al.*, Scikit-learn: Machine Learning in Python, *J. Mach. Learn. Res.*, 2011, **12**, 2825–2830.
50 F. Allegrini and A. C. Olivieri, IUPAC-Consistent Approach to the Limit of Detection in Partial Least-Squares Calibration, *Anal. Chem.*, 2014, **86**(15), 7858–7866, DOI: 10.1021/ac501786u.
51 C. Méndez-López, L. Javier Fernández-Menéndez, C. González-Gago, *et al.*, Novel optical method based on nebulization assisted laser induced plasma on inexpensive paper substrates for online determination of halogens and metals in liquid samples, *Opt Laser. Technol.*, 2023, **164**, 109536, DOI: 10.1016/j.optlastec.2023.109536.
52 C. Méndez-López, L. J. Fernández-Menéndez, C. González-Gago, *et al.*, Nebulization assisted molecular LIBS for sensitive and fast fluorine determination in aqueous solutions, *J. Anal. At. Spectrom.*, 2023, **38**(1), 80–89, DOI: 10.1039/d2ja00319h.
53 K. Neubauer, Calibration: Effects on Accuracy and Detection Limits in Atomic Spectroscopy, *Spectroscopy*, 2021, **36**, 14–16.